

University of Massachusetts Boston
ScholarWorks at UMass Boston

Graduate Masters Theses

Doctoral Dissertations and Masters Theses


12-31-2015

Automatic Detection and Quantification of Bluff Erosion Events in Single Image Series

Martin D. Hellwig

University of Massachusetts Boston

Follow this and additional works at: http://scholarworks.umb.edu/masters_theses

 Part of the [Computer Sciences Commons](#), [Environmental Sciences Commons](#), and the [Geomorphology Commons](#)

Recommended Citation

Hellwig, Martin D., "Automatic Detection and Quantification of Bluff Erosion Events in Single Image Series" (2015). *Graduate Masters Theses*. Paper 352.

This Open Access Thesis is brought to you for free and open access by the Doctoral Dissertations and Masters Theses at ScholarWorks at UMass Boston. It has been accepted for inclusion in Graduate Masters Theses by an authorized administrator of ScholarWorks at UMass Boston. For more information, please contact library.uasc@umb.edu.

AUTOMATIC DETECTION AND QUANTIFICATION OF
BLUFF EROSION EVENTS IN SINGLE IMAGE SERIES

A Thesis Presented

by

MARTIN D. HELLWIG

Submitted to the Office of Graduate Studies,
University of Massachusetts Boston
in partial fulfillment of the requirements for the degree of

MASTER OF SCIENCE

December 2015

Computer Science Program

© 2015 Martin D. Hellwig
All rights reserved

AUTOMATIC DETECTION AND QUANTIFICATION OF
BLUFF EROSION EVENTS IN SINGLE IMAGE SERIES

A Thesis Presented

by

MARTIN D. HELLWIG

Approved as to style and content by:

Marc Pomplun, Professor
Chairperson of Committee

Craig Yu, Assistant Professor
Member

Dan Simovici, Professor
Member

Dan Simovici, Graduate Program Director
Computer Science Program

ABSTRACT

AUTOMATIC DETECTION AND QUANTIFICATION OF BLUFF EROSION EVENTS IN SINGLE IMAGE SERIES

December 2015

Martin D. Hellwig, Dipl. Kfm., Luneburg University
MBA, University of North Dakota
M.Sc. University of North Dakota
M.Sc. University of Massachusetts Boston

Directed by Professor Marc Pomplun

Many communities along coastlines and riverbanks are threatened by water erosion and hence an accurate model to predict erosion events is needed in order to plan mitigation strategies. Such models need to rely on readily available meteorological data that may or may not be correlated with the occurrence of erosion events. In order to accurately study these potential correlations, researchers need a quantified time series index indicating the occurrence and magnitude of erosion in the studied area. We show that such an index can be obtained by creating and analyzing a single image series using relatively cheap consumer grade digital cameras. These image series are naturally of lower quality and subject to a large amount of variability

as environmental conditions change over time. We initially analyze each image as a whole and subsequently demonstrate the great advantages of segmenting each image. This allows for independent parallel processing of segments while preventing cross-contamination between them. Finally, we are able to automatically detect 67% of all erosion events while accepting only a small number of false positives.

TABLE OF CONTENTS

ABSTRACT.....	iv
LIST OF FIGURES	viii
LIST OF TABLES	ix
CHAPTER	Page
1. INTRODUCTION	1
2. METHODOLOGY	6
Data	6
Whole Image Approach	7
Recurring Changes	8
Short Term Averages	10
Color Channel Omissions	12
Edge Detection.....	15
Changes.....	17
Results.....	17
Image Segmentation.....	18
Robustness	18
Recursive Segmentation.....	20
Parallelizability	22
Segment Procedure	24
Segment Preparation	24
Temporary Disturbances	25
Changing Lighting Conditions.....	26

Image Comparison	27
Index Generation.....	29
Reassembling the Image	30
3. RESULTS	33
Plottable Index	33
Accuracy	34
Statistical Significance.....	36
4. DISCUSSION.....	38
Results.....	38
Application.....	39
Further Research	39
BIBLIOGRAPHY	41

LIST OF FIGURES

Figure	Page
1: Recurring Changes Caused By Wave Motion	8
2: Image Mask.....	9
3: Mask Applied to Frequently Changing Areas	10
4: Short Term Average.....	11
5: Preprocessing Options	14
6: Edge Matrix	16
7: Original Sobel.....	17
8: Best Change Matrix	18
9: Average Change Matrix.....	18
10: Segmentation Into 120px Squares	21
11: Segmentation Into 60px Squares	22
12: Assembled Change Matrix.....	28
13: Source Images Used.....	28
14: Change Indices.....	31
15: Interpolated Erosion Index Graph.....	32
16: Erosion Index and Wind Gusts	34
17: Example of a False Positive.....	36

LIST OF TABLES

Table	Page
1: Actual Erosion Events	35
2: False Positives.....	35
3: Statistical Significance.....	37

CHAPTER I

INTRODUCTION

Life as we know it relies on a number of fundamental resources: clean air, water and food. The production of ample food is itself most reliant on the availability of air and water which allows us to consider these two to be sufficient essential requirements for any successful settlement. It is, then, not surprising that historically most villages, towns and cities developed along natural water sources such as lakes, rivers and, of course, the oceans' shorelines (Lucero, Fedick, Dunning, Lentz, & Scarborough, 2014). Clean air was typically not in short supply so bodies of water attracted human settlement not only due to their inherent life sustaining properties but also the ability to serve as trade and transport routes. However, as much as water has helped to attract and sustain human settlements, it has also always posed a certain threat to them (C. C. Huang et al., 2010). Flooding may be the most obvious of these threats and researchers have been trying to accurately calculate flood risk and forecast specific events for a long time, often using indirectly related data (Caradot, Granger, Chapgier, Cherqui, & Chocat, 2011) . Many communities, such as those in the Rhine delta, have accrued significant expertise mitigating flood risk using large scale dams and flood gates (Protection & Brown, 2008).

However, some of these installations may not suffice to combat the increased flood risk created by climate change patterns. Similarly, new mitigation efforts will have to take these new requirements into account to assure reliability of the management and mitigation efforts (Karamouz & Nazif, 2013).

Aside from major flooding events, erosion is a more subtle yet equally important threat (Spaan, Winteraeken, & Riksen, 2006). Constant water erosion can weaken or eliminate natural flood protection zones and often threaten human settlements directly (Islam, Sallu, Hubacek, & Paavola, 2014). This is particularly common in bluff erosion cases that quite literally wash out the ground from under existing coastal communities (Buckler & Winters, 1983). A wide range of engineering solutions offer protection from water impact and the resulting erosive effects (Beilicci, Beilicci, & Ștefanescu, 2014). On coast lines, these can include basic wave breakers as well as sea wall reinforcements using materials such as concrete or granite blocks. Particularly threatened communities may resort to more sophisticated mitigation strategies such as artificial dune construction (Matias, Ferreira, Mendes, Dias, & Vila-Concejo, 2005). In some cases previously reclaimed land is purposely designated as flood land to reduce the effects on point further inland (van Staveren, Warner, van Tatenhove, & Wester, 2014). Natural flood protection zones have also proven to be effective in many cases (Schmitt, Albers, Pham, & Dinh, 2013).

Even when human dwellings are not directly impacted, excessive erosion can affect existing infrastructure and threaten local economies, notably those relying on

tourism (A. Smith, 1995). From a conservational perspective, many bluff areas are also prime habitats for many endangered species (Carpenter, Jung, & Sites Jr, 2001).

Erosion management is typically quite expensive and many methods might not be effective when applied in the wrong location or at the wrong time (Paterson et al., 1993). Therefore, an accurate erosion forecast would be extremely helpful in assuring an efficient and effective erosion prevention effort. In addition to prevention, affected communities would also be able to prepare needed resources to respond to unavoidable erosion events if they could reasonably anticipate the timing and scope of erosion events (National Oceanic and Atmospheric Administration, 1998).

Water erosion is highly dependent on environmental and meteorological conditions as well as the geomorphic composition of the existing soil (Castedo, Fernández, Trenhaile, & Paredes, 2013). In addition, the local geography and oceanography (Jorgenson & Brown, 2005) play a major role in erosion patterns and introduces a large enough variability to make a general forecast model impossible (Dawson & Evans, 2001). Instead, any good erosion forecast has to rely on a substantial amount of past observation from the specific area for which a forecast is sought. Similarly, only local present observations can assure the accuracy of any forecast based on such a model (Barsanti et al., 2011).

Creating the actual forecast model will be an interesting Machine Learning topic. We may address this in a future study. Within the scope of this work, we will aim to analyze automated observations in a fashion that allows us to detect and quantify erosion

events. We will establish an erosion index that can later be correlated with meteorological data to detect patterns and automatically generate a forecast model for the observed area.

Bluff erosion can be measured using a wide variety of advanced tools including aerial photography (Day, Gran, Belmont, & Wawrzyniec, 2013b) or satellite based Geographic Information System (GIS) data (Dabojani, Mithun, & Kanti, 2014). The accuracy of either approach may be significantly improved using additional remote sensing technologies including terrestrial laser scanning (Day, Gran, Belmont, & Wawrzyniec, 2013a). This method has also been successfully applied to avalanche modeling (Prokop et al., 2015). Wave load analysis tends to be quite reliable as basis for erosion forecasts as well (Soomere, Viška, Lapinskis, & Räämet, 2011), but it only allows for short term predictions.

Within this study we will concentrate on single stationary cameras which present a much more readily available source of observations. Many of the more advanced monitoring tools can be financially demanding while simple cameras are comparably affordable and relatively easy to install. In addition, many existing webcams provide freely available image series that may be used for analyses although typically the quality of dedicated devices is much superior and hence preferable.

Our analysis will focus on a series of images obtained from one single camera and attempt to extract a time series of erosion indices. This analysis is particularly challenging as it has to automatically account for the at times extreme variability that is inherently present in such image series of natural features (Lalonde, Efros, & Narasimhan, 2012). Examples of interferences include changing positions of the sun,

varying lengths of the days throughout the observation period, irregular weather patterns, etc.

After accounting for these natural contaminations, we will develop a method to detect soil erosion by adapting classic motion detection algorithms (Dupret, Verdant, Villard, & Mathias, 2011) to detect medium term changes in image series. We need to pay particular attention to gradual changes that happen over time and are not recurring events (Li, Han, Lin, & Wei, 2012) as the latter are highly unlikely to be signs of erosion. Erosion is – by definition – irreversible and should hence not be recurring.

Finally we develop an adapted quantifying mechanism (Paganelli, Peroni, Baroni, & Riboldi, 2013) that will allow us to generate the aforementioned erosion index.

CHAPTER II

METHODOLOGY

Data

Data acquisition for this study was conducted in cooperation with the Coastal Environmental Sensor Network (CESN), the National Park Service (NPS) and the Thompson Island Outward Bound Education Center (TIOBEC). CESN operates a wide variety of environmental sensors and cameras on several of the Boston Harbor Islands (BHI). We are focusing on data from Thompson Island, specifically a bluff camera positioned at the northern tip of the island. This camera provides still images in five minute intervals during one hour before and one hour after each high tide. In this fashion, twenty four images are collected per tide cycle. Images from nighttime high tides are discarded as they would not provide any reasonable amount of information.

In addition to the mentioned series of still images monitoring the northern bluff, we also have the coinciding environmental data collected by TIOBEC's weather station on Thompson Island available. This data will become more important as future studies will aim to create an actual forecast model.

Whole Image Approach

During the course of evolution, humans have developed the ability to focus on important pieces of information in images while paying less attention to or entirely ignoring areas that are of no concern (Kastner & Ungerleider, 2000). Through the process of natural selection the species has also become quite good at detecting motion (An, Gong, McLoughlin, Yang, & Wang, 2014). As a result, human subjects are able to compare two images showing the same scenery and quite easily point out small areas of change (Párraga, Troscianko, & Tolhurst, 2005) - even when a lot of unrelated change occurs in the remaining image (Kinsey, Anderson, Hadjipapas, & Holliday, 2011). This allows them to quickly observe and report erosion events in an image series.

In Computer Vision, researchers do not have the luxury of working with hardware that has developed any such survival skills. In order to automatically detect occurring erosion in the given image series, we must develop a method to filter out noise before our algorithm can successfully find and quantify erosion events.

To solve this problem, we can either consider each image in its entirety or instead decide to split each image into smaller pieces and analyze them individually (Zhongli, Xiumei, & Jie, 2014). The whole image approach will require substantially more preprocessing but may provide the best results for erosion detection as it allows us to consider each change in a broader context (Aleksandrowicz, Turlej, Lewiński, & Bochenek, 2014). Let us therefore begin by analyzing each image in the series in its entirety.

Recurring Changes

Our images series contains excellent examples of frequently recurring motion that would be detected by any motion or change detection algorithm the same way that actual erosion would be detected. Wave motion, shown in Figure 1, is an important example of such repetitive motion.



Figure 1: Recurring Changes Caused By Wave Motion

In order to limit these false positives, one needs to determine areas of particular volatility in the images (Cheng & Buckles, 2014) so that they may be excluded from any further analysis. We achieve this by first parsing every image and extracting the red, green and blue channels. This allows us to create average values for each pixel and each channel over the entire set of images. In effect, this creates an average image (Bisquert et al., 2015).

As a second step we compare each individual image against the average and calculate the distance of each pixel and channel between the average image and the inspected one. This gives us a difference matrix which will also be averaged out over the entire series of images (Eivazi, Kolesnikov, Junttila, & Kauranne, 2015). We can use this

average variability matrix as a mask to ignore overly dynamic areas in the images. In our example we used a threshold value of 200. This means that if the combined average variability of a given pixel amounts to more than 200 across the three color channels, it is considered unreliable for our purposes and hence becomes a black pixel (0) in the black and white mask illustrated in figure 2. This arbitrary threshold may later need to be replaced by a dynamic value created by a machine learning algorithm.



Figure 2: Image Mask

Finally, we use this mask image and multiply it with each original image to obtain a series of masked images in which only reasonably constant pixels remain while those with high variability are replaced with black pixels (Fisher, 2013). As this operation is performed on every image, our subsequent change detection will not be affected by them. Figure 3 shows that most of the wave motion has been removed. We will deal with the relatively small remaining areas in a later step.



Figure 3: Mask Applied to Frequently Changing Areas

As this example illustrates, likely areas filtered out by this method include tidal waters as well as the sky – neither of which are of interest for the erosion analysis. In this fashion we not only decontaminate the images, but also reduce the amount of unnecessary information which can likely provide performance gains in real life applications relying on larger sample sets (Kastens et al., 2005).

Short Term Averages

Erosion is a relatively slow process and we are most interested in the occurrence of major events. Such major changes in soil configuration may well be the sum of multiple smaller erosions that happen during the same individual observation frame (Moura et al., 2012), yet for the further studies the exact time of each event will not be relevant. We therefore need not compare each of the 24 images during any given observation frame. Reducing the number of comparisons is not only computationally beneficial, but it also greatly assists with a significant problem posed by changing lighting and weather conditions.

As the sun's position in the sky changes throughout each two hour observation frame, the lighting conditions will vary independently of any other noise in the images. As solar positions are perfectly predictable (Lai et al., 2015), one could consider calculating and adjusting for the different illuminations. This, however would be somewhat expensive and also would only solve one part of the lighting problem. As the sample data was obtained using nonscientific equipment, changing solar angles create secondary noise such as glare and reflections which are much harder to correct for (Ashique & Kaliyadan, 2011). This problem is exacerbated when one takes the reflective properties of moving water surfaces into account.

But, as previously stated, this granularity is not actually needed. It will be sufficient to report change between observation frames or partial frames. We achieve this by simply merging a given number of sequential images from the same observation frame into one image that can be used for further analysis.

When merging images, one typically needs to account for minor camera movements (Yue, Cai, Luo, Jin, & Zeng, 2015). The example in figure 4 contains considerable camera motion that is represented by a slight blur. This, however, will not significantly affect the further analysis as our focus is on larger change events meaning that we can safely sacrifice smaller feature detail in order to optimize the procedure.



Figure 4: Short Term Average

In this fashion we drastically reduce the number of images in the data set which will also save computing time later on. The exact aggregation ratio might be automatically optimized at a later stage while for our initial analysis a maximum of two images per observation frame will be used. In either case, ratios may vary as data sources will typically be incomplete. In order to deal with missing images, we simply select all images from any given frame and merge up to twelve of them into a new sample. Whenever more than twelve are available, they will be evenly split between merged samples.

By creating such aggregates, short term changes in the image become less prominent (Benabbas, Ihaddadene, & Djeraba, 2011). Disturbances such as glare will be visible, but unless they happen to occur in the same location in each source image, they will be less dominant and hence less problematic during our further analysis. In this situation solar motion actually works to our advantage as it virtually guarantees that glare and undesirable reflections will not be in the same area of multiple images.

Color Channel Omissions

The CESN camera provides RGB images, meaning that it provides a full byte of brightness data for each color channel and for each pixel. In order to simplify the further processing, this breadth of information needs to be reduced to a narrower, more applicable scope. To achieve this, there are essentially three options:

- a) Convert the image to grey scale, effectively averaging the three color channels and producing a single intensity value for each pixel. This option would cut the amount of information to 1/3 and most features in the image will still be

detectable as figure 5 illustrates. However, color changes will be less prominent or may be entirely obscured if the overall intensity remains unchanged (Yoonessi & Zaidi, 2010).

- b) Convert images to HIS color space. In this case we could specifically analyze color changes while ignoring lighting induced changes in intensity. HIS is known to better represent many natural features (Ondimu & Murase, 2008). However, converting images takes considerable time (Nnolim, 2015).
- c) Split the color channels and potentially omit one or two of them. This might be particularly useful in bluff erosion situations as soils tend to be quite rich in red and green tones while blue may not be as important in determining changing ground configurations (García-Mateos, Hernández-Hernández, Escarabajal-Henarejos, Jaén-Terrones, & Molina-Martínez, 2015).

Figure 5 shows a comparison between the an original sample image and its preprocessed counterparts. It is fairly evident that the approach using an HSI decomposition with subsequent intensity masking and recomposition is not as usable as hoped. Due to the high compression ratio in our original images, we generate a large number of unwanted edges and obtain an image of unacceptably low quality for further processing. At the same time it appears that in many cases hue and saturation do not vary across the source image as much as anticipated which means that we must maintain intensity values as well. This, unfortunately, eliminates the HSI approach.

There is a noticeable difference in clarity between the two grey scale versions of the image. As expected, omitting the blue channel did provide better contrast. In this

example the last option even appears better suited for further analysis than the original image. While this cannot be assumed to be the case for all instances, we are confident that in no case should it generate notably inferior results. Considering the much lower processing time for a grey scale image versus an RGB image, we should therefore proceed with this grey scale image that was generated by averaging the original image's red and green channels.

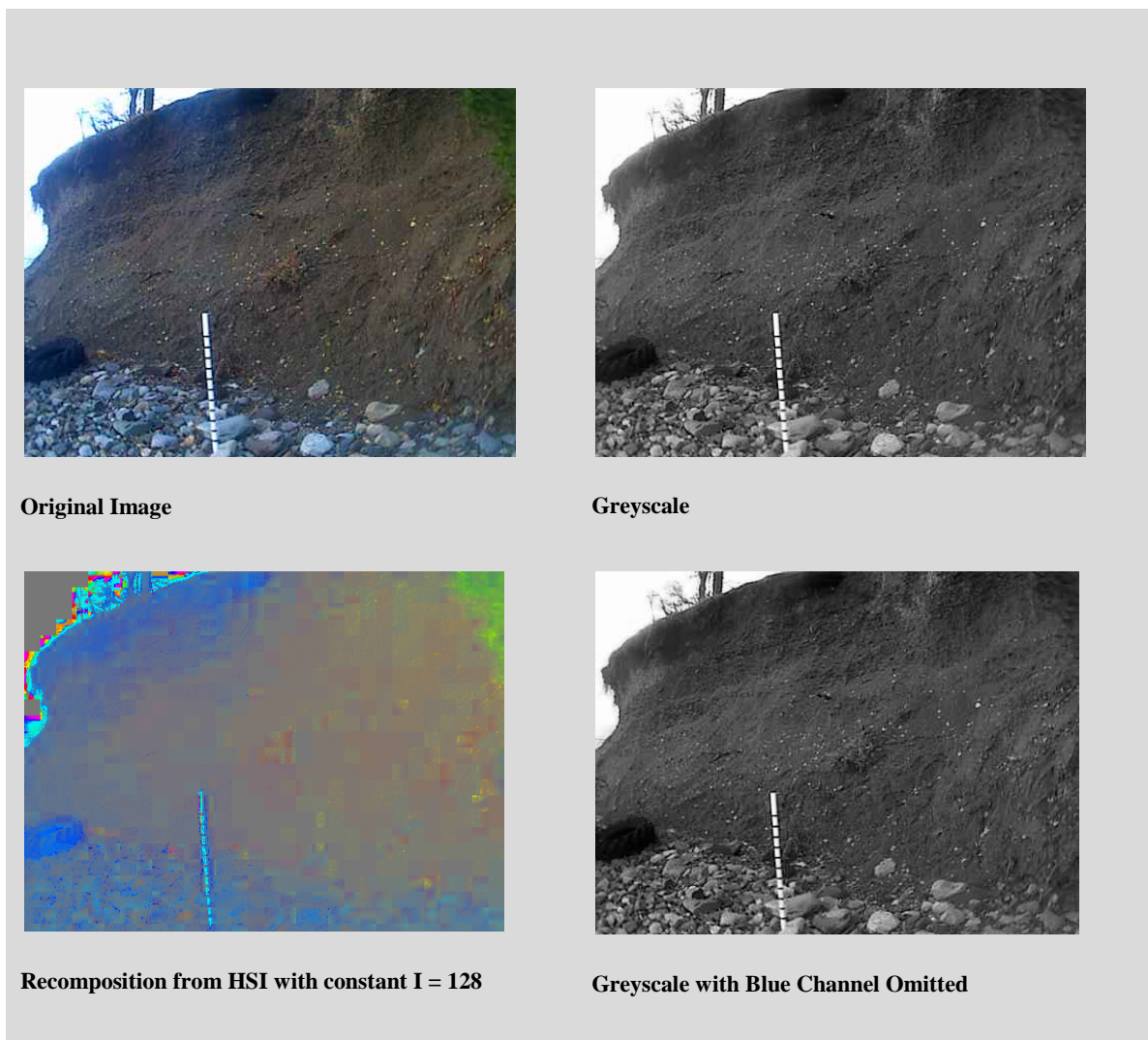


Figure 5: Preprocessing Options

Edge Detection

Erosion is – by definition – characterized by a shift in soil contours (Steudel et al., 2015). To find such shifts, we must first find said contours in our images. This can be accomplished using a wide variety of edge detection algorithms (Y. Wang, Wang, & LIU, 2003). This study uses a modified Sobel filter that allows us to detect horizontal and vertical edges separately (Singh et al., 2014). In the case of bluffs, virtually all erosion will be expressed by slumping soil that will result in changes of horizontal boundaries. Vertical edges may also change as slump scars occur (D. P. Smith, Ruiz, Kvitek, & Lampietro, 2005), but they can be ignored as they are not dominant indicators (Boak & Turner, 2005). In fact, they will almost always be accompanied by horizontal motion (da Silva, Huang, Francesconi, Saintil, & Villegas, 2015).

Consequently we are most interested in horizontal edges which may be detected using just a part of the Sobel algorithm. The regular Sobel filters detect vertical and horizontal edges separately and then calculate the overall edge intensity as the square root of the sum of the squared individual filters (Singh et al., 2014). Our much simpler strategy employs only the horizontal filter. However, edges in images of natural soil will always be relatively smooth and edge strength has been further deteriorated by image averaging during the antecedent preprocessing steps.

Rather than relying on the six neighboring pixels above and below (pixels to the left and right are obviously ignored in a horizontal edge detection), we will use six additional pixels – three from two rows above and three from two rows below. The resulting matrix will help us better assess horizontal edge strength in a smoothed image.

Using such a large filter has the negative effect of reducing the usable image size. We lose two rows on the top margin, two rows on the bottom margin and two columns each on the left and right image margins. In a 480*360px image, 3344 pixels or about 1.9% of the overall image are hence sacrificed. We can reasonably accept this loss of information as it is very likely that the most interesting features will be found closer to the images center. This assumption is based on the fact that cameras will typically be aimed at whatever feature is of most interest to the individual operator.

A larger convolution matrix also has the added disadvantage of significantly increasing computational requirements. The Sobel filter only requires six multiplications per pixel while our modified matrix requires twice as many.

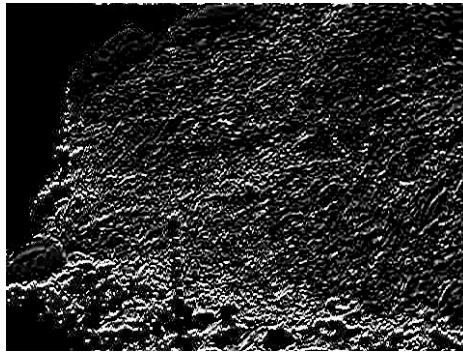


Figure 6: Edge Matrix

Figure 6 shows the masked edge matrix for the image introduced in figure 5. One can clearly see a large number of well defined horizontal edges. Compared to an edge matrix computed from the original image using a traditional Sobel filter (Figure 7), this is a considerable improvement. However, the nature of the image results in an undesirably high number of edges that are quite close to each other. This will negatively influence our motion detection as moving edges will overlap and hence be undetectable to any algorithm that relies on change matrices.

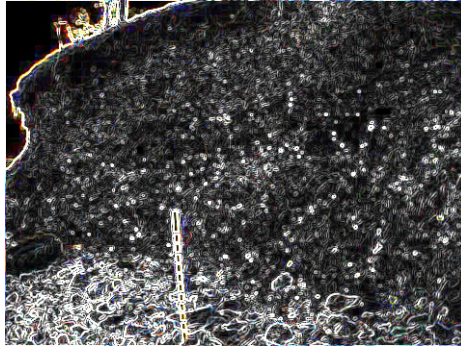


Figure 7: Original Sobel

Changes

We are interested in erosion events that will be expressed as changes between two observation periods. Each of these periods is now expressed by an edge image that we can use to detect any changes that may have occurred between two periods. Only comparing neighboring observations allows us to simply subtract one edge image from its successor. Working with grey scale, this will yield a matrix with pixel values ranging from -255 to +255. The sign of the values is dependent on the order in which the images are processed, but has no significant impact on our further analysis. We can therefore simply replace any negative value with its positive counterpart. This has the added benefit of strengthening change areas as both the previous and the new edge will be highlighted in the change matrix. Figure 8 show the strongest image over image change that this method detected.

Results

As figure 8 illustrates, even the strongest change detected still appears quite weak. This is a result of the substantial information loss caused by the intensive preprocessing required by the heterogeneity of the sample image series. Deteriorated images yielded

edge matrices of limited utility which ultimately resulted in an almost entirely black average change matrix shown in figure 9.

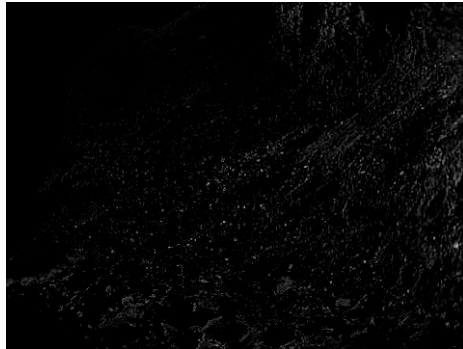


Figure 8: Best Change Matrix

It appears evident that these results are not usable. In fact, none of our attempts to quantify occurred changes yielded much better results than a random generated control. Consequently we must abandon the whole image approach and seek a better method of erosion detection and quantification.

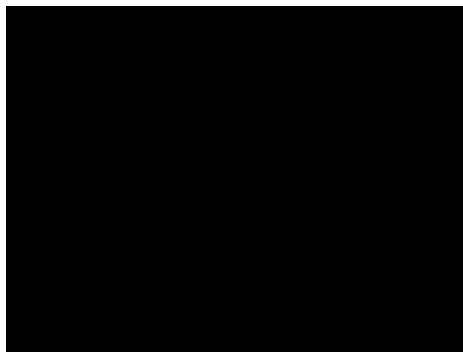


Figure 9: Average Change Matrix

Image Segmentation

Robustness

As previously demonstrated, detecting erosion in series of natural images can be challenging. The constantly changing environmental conditions induce a large variability into image quality and the amount of information available in each image. We have

introduced a number of different strategies to counteract this variability but have also determined that in many cases certain areas of the image show very different changes than others. Consequently our response to a bright streak of sunlight in one half of an image may destroy perfectly usable information in other areas. Masking particularly volatile pixels or areas has reduced but not eliminated this issue.

Since different areas of the image appear to change independently of each other, one needs to consider an alternate approach under which each independent area is analyzed separately. In this fashion corrective actions on one particular part of an image can safely be performed without negatively affecting any other area (Liau, 2014).

In order to separately analyze particular regions within a given image, we must first determine a method to define such regions and separate the entire image into corresponding segments. As this study observes change over time, the segmentation will be identical for all images throughout the entire series.

One possible approach would involve manual segmentation based on areas of interest. This is undoubtedly the most effective method as we could intelligently create heteromorphic regions based on preexisting observations. This manual preprocessing does, however, introduce complexity into the procedure of performing erosion detection in the field. It would require calibration each time a new observation is started and prevent easy adaptation to new cameras or locations. Therefore, the employed segmentation method must handle any image automatically and determine the areas of interest by itself.

However, automatic dynamic segmentation using any of the numerous common algorithms (S. Zhu, Zhao, Guo, & Zhang, 2013) proves mostly impossible as our images are naturally rich in non-gaussian noise which these algorithms are generally incapable of handling (Tenbrinck & Jiang, 2015). Principal component analysis is bound to fail due to the fact that there are no sufficiently significant objects. Virtually all erosion events happen in the image's background (Dronova, Gong, Wang, & Zhong, 2015).

Finally let us consider the option of segmenting the image using a static segmentation grid. As we will compare each pair of subsequent images in the series and attempt to detect erosion that occurred in the time span that passed between the moments the images were captured, this is a viable solution. It will automatically detect areas of interest, even if segments are defined somewhat arbitrarily (Z. Zhu & Wang, 2012). In order to facilitate further processing we avoid complex shapes and instead split the original image into a set of equally sized squares that can easily be processed separately.

Recursive Segmentation

Images can easily be broken into a given number of squares or into the most appropriate number of squares of a given size. Alternatively, we can recursively break down the image into smaller and smaller subsegments (Tang, Mu, Zhao, & Zhao, 2014) until a segment size of one pixel is reached. Each segment would subsequently be analyzed independently and then aggregated back into an analysis of each pair of whole images (Teng & Chang, 2012).

This would, of course, minimize the theoretical runtime using a parallel computing approach. However, while segmentation helps us to reduce the adverse effects

of erratic changes in one segment on others, erosion cannot be detected at the pixel level. By definition erosion occurs in areas as soil moves and changes in individual pixels are not suitable for motion detection in a given neighborhood. Therefore, a certain minimum segment size must be maintained in order to detect any change that might represent soil motion and hence indicate an erosion event. It can be expected that the optimal segment size will vary between different image series and observed land features. However, as previously eluded to, we do not aim to achieve the optimal solution for any one given case, but rather a usable solution that will apply to a larger number of general cases. We will therefore begin with a segment size of 120*120 pixels, breaking down our sample set into the twelve segments shown in figure 10.



Figure 10: Segmentation into 120px squares

The differences between the quadrants are immediately apparent. Some have large proportions of sky. some are likely to see tidal fluctuations and others represent various segments of soil. It is important to note that this distribution is not the result of experiment design but rather an inherent feature of the segmented image set. The same

approach will therefore work for a wide range of image series although the individual segments will obviously play very different roles when derived from other data sources.

As previously discussed, we could employ a finer grid and split each image up into more individual segments. Consider the example of 48 segments in figure 11, each 60*60 pixels in size. Obviously the segmentation and separation of different image contexts improves.

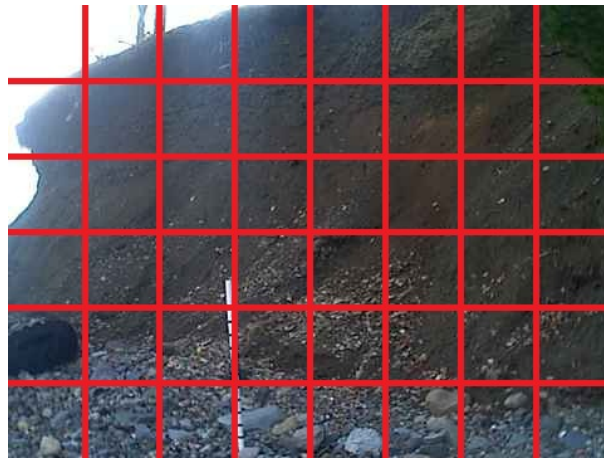


Figure 11: Segmentation into 60px quares

However, this step necessarily also narrows the observational focus to a much smaller area within which motion of individual leaves might be detected more accurately than soil slumping that may occur throughout a number of neighboring squares. In our further analysis we will therefore mainly use 120*120px.

Parallelizability

By breaking down each image in the original series into multiple segments, we are creating a separate image series for each one of those segments. As a result our final

solution produces 12 separate series of evenly sized images and each one of these series must be prepared and processed separately. As the overall number of pixels across all segments does not increase in the segmentation procedure, the overall computational requirements are only increased by the overhead needed for segmentation and final reassembly of the data. However, these two steps are relatively cheap by comparison and hence do not significantly increase the procedure's final runtime (Bejinariu, Costin, Rotaru, Luca, & Nit, 2014).

While runtime will marginally increase, memory requirements decrease drastically as we can process smaller chunks of images sequentially rather than having to keep multiple sets of large images in memory to allow for the comparison based motion detection. This will allow this approach to run on smaller and less powerful hardware platforms.

The same effect also makes the entire procedure highly parallelizable (L. Wang, Ma, Zomaya, Ranjan, & Chen, 2015). As each segmented image series can be processed independently of all others, we can easily process multiple series on any available processors or cores. It is, of course, likely that researcher implementing the work laid out in this thesis would not have sufficient cores available to assign each segment to its own core - particularly when working with larger images and/or very small segments. Hence a series parallel processing approach will yield the best performance and lowest overall runtime.

Said runtime is, of course, heavily dependent on the original image series as the number of necessary comparisons will vary among different image qualities. It is

therefore not trivial to estimate the exact time the procedure will need for a given input size. It is, however, quite evident that segmenting the image creates immense parallelization opportunities which will reduce the time needed to detect motion and compute the overall erosion index.

Segment Procedure

Even using our small sample sizes, available computing resources are already a limiting factor. It is therefore imperative that image segmentation and segment analysis are performed in an efficient manner (L. Wang et al., 2015). We cannot afford to simply load the entire sample series into memory and selectively read and analyze each individual segment. Instead, each thread will be designed to only handle a very limited number of small image segments at any given time. To accomplish this, we sequentially load each sample image, create the appropriate number of segments and store them on the file system. In our initial case of 120*120px segments, this creates twelve separate series of segments.

Segment Preparation

Our primary goal in the image segmentation approach is the isolation of disruptive change that occurs in individual areas of the image. Such change might be caused by sunlight, changing tides or particularly unstable landscape features such as moving tree branches.

Our previous whole-image-approach used a two pronged approach to this problem. We chose to ignore any image that deviated too far from the average and further

introduced the concept of masking. The latter process specifically addresses areas of excessive change throughout the entire observation period.

The segmented approach still needs to filter out outliers in the original series, but the individual segments also allow us to implement a more robust volatility handling than the aforementioned masking. By considering only a small part of the image, we can simply ignore any instance that shows excessive change from its predecessor in the series. This was impossible using the whole image as a large number of images show excessive change in one small area while other areas are perfectly usable and might well contain important information. Ignoring just an individual segment that seems to be changing too fast will maintain that useful information while eliminating the harmful influence caused by an individual feature.

Temporary Disturbances

In some cases indicators of actual change may be hidden under a stronger signal caused by a temporary disturbance. For example, a particularly high tide might inundate parts of the bluff and then retreat to expose significant erosion. Simply ignoring the obviously excessive change from brown soil to white water presents the risk of missing the erosion effect altogether (Jia et al., 2011). In order to avoid this dilemma, a cascading comparison will be invoked whenever excessive change is detected. If a particular segment instance is deemed unusable, we will compare its predecessor to its successor instead and continue this procedure until the next sufficiently similar image is found or until a predefined threshold is reached. In this fashion we effectively interpolate missing data (Ayana, Worqlul, & Steenhuis, 2015) and greatly increase our chances of comparing

a segment photographed before a temporary disturbance to one that was taken afterwards. This procedure can thus detect change that occurs during such a disturbance. The accuracy of the event's timing naturally decreases, but this is clearly preferable over losing the event information altogether.

Changing Lighting Conditions

Even rather stable landscape features will be subject to varying lighting conditions that can introduce false positives into our motion detection attempts. While we have had limited success addressing this issue in the whole-image scope, working with individual segments allows us to adjust each individual area much more appropriately. The approach, however, remains largely unchanged. We generate an average image over the entire segment series, compute each individual segment's average deviation from that whole series average and stretch or compress each color channel individually in order to counteract lighting change that may have occurred throughout the entire segment (Dutta, Leahy, & Li, 2013). As neighboring instances within the segment series will all be subjected to the same treatment with respect to the same series average, all significant features will be maintained, allowing for higher sensitivity motion detection without losing pertaining information about items that may have shifted (Guo, Rage, & Ninomiya, 2013).

After adjusting for changing light conditions, we must also create a new average image. This will naturally be much smoother than the original average image and provide a substantially more reliable basis for detection and handling of outliers in the subsequent difference analysis.

Image Comparison

As previously eluded to, each image is compared to its predecessor or - in certain cases - with an image farther back in the timeline. In order to detect change between the two samples, we simply compute the absolute difference between each of the three color channels and average the resulting change to create an overall change matrix. Each processed image will result in a separate change matrix of identical size that represents lack of change by black pixels and increasing levels of change by lighter shades of grey. A white pixel in the change matrix hence implies that in one of the two sample images the corresponding pixel must have been white while in the other image that same pixel must have been black as this is the largest theoretically possible change between the two (Portillo-Portillo, Sánchez-Pérez, Olivares-Mercado, & Pérez-Meana, 2014).

During the actual comparison we will reject any successor that represents an excessive change and proceed to the nearest subsequent image that can be used for a more reliable comparison. In most cases we consider the top 25% strongest sample over sample changes within each segment to be excessive. This step implements the elimination of temporary disturbances discussed in an earlier chapter. Figure 12 shows an array of resulting change matrices. Two segments at the bottom left corner were ignored as the change occurring there was considered excessive. The source images in figure 13 reveal that this change was caused by moving water which indeed should be ignored for our purposes.

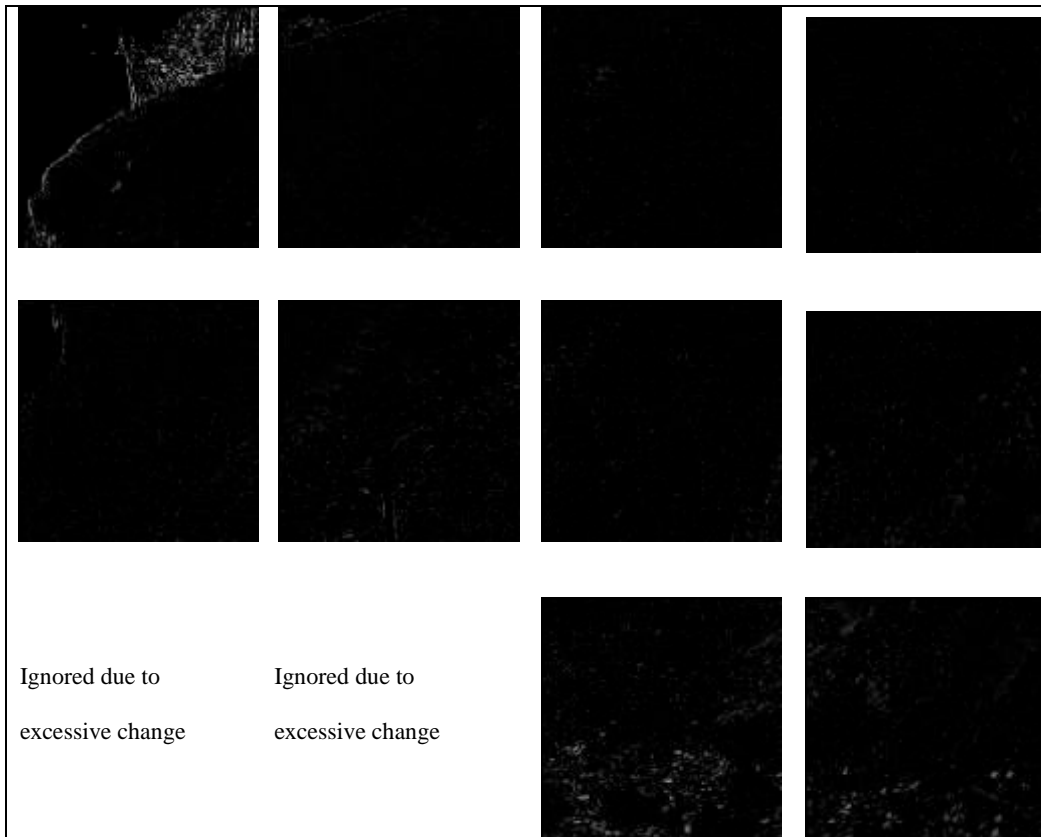


Figure 12: Assembled Change Matrix

The same images also show a very distinct erosion event in the bottom right corner which is well represented in our change matrices. We still have an undesirably strong signal in the upper left corner, where changing lighting conditions result in a false positive that will negatively influence the accuracy of our desired erosion index.



Figure 13: Source Images Used

Index Generation

After creating a series of change matrices, we can compute a change index for each of the underlying observation frames. Any such index has to be designed to detect particular types of changes. In our case we aim to detect erosion events which tend to be localized within the image. They are also expected to have a certain continuity as erosive slumps typically affect a significant area and do not leave interspersed features unchanged.

Consequently this erosion index has to amplify smaller regions of connected change activity while squelching random changes observed throughout the entire image. Such indices are widely used for purposes such as building change detection (X. Huang, Zhu, Zhang, & Tang, 2014) or vegetation change monitoring (Vicente-Serrano et al., 2015). Some algorithms make use of different refractive properties of moving objects (Rozanov, 2004). This, however, will not be useful in our case as we are monitoring soil with rather homogeneous refractive values (Peltoniemi, Hakala, Suomalainen, & Puttonen, 2009).

It would be possible to parse each change matrix for bright pixels and subsequently analyze the size of each connected area of interest. This would undoubtedly yield the best results, but it would at the same time be very expensive in computational terms. In order to reduce infrastructure requirements, we will instead rely on the fact that change areas tend to be brighter - or more intense - at their centers while the outer perimeters are often weaker. Excessive change events were already filtered out in a prior step which assures that at the index generation step, the brightest spots will represent the

most significant change events in the image. We can hence simplify our index generation and simply assign a higher weight to particularly bright spots. This is achieved by computing the root mean cubed intensity using the following simple formula:

$$I = \frac{1}{XY} * \sqrt{\sum_{x=1}^X \sum_{y=1}^Y P_{x,y}^3}$$

where $P_{x,y}$ is the intensity of the pixel at coordinates x,y

We use a cubed intensity value as the change matrices obtained during the change detection phase are generally relatively dark and the few bright spots scattered throughout them are most likely to indicate localized change. Large scale minor changes may be represented by larger numbers of low intensity grey pixels throughout the entire matrix which receive a much lower weight using this method.

Reassembling the Image

The described method yields a set of up to twelve change indices per image. Our previous example from figure 13 shows moderate washout in the bottom right corner. At the same time the observer will notice the much more noticeable - although irrelevant - recession of the tidal water on the lower left side.

Our change indices in figure 14 clearly indicate the areas of relevant change while ignoring the water's motion on the left. In this visualization indices over 65 are colored red while missing figures indicate ignored change indices.



Figure 14: Change Indices

While this example highlights the capabilities of our approach, it also includes a counterexample in which a very high index was computed for the top left segment due to the changing lighting conditions in this area. These changes were not excessive enough to be filtered out during the generation of the change matrices, but clearly overpower the remaining individual segment indices. We must expect such residual disturbances to occur intermittently and hence deploy a robust method that will create a reliable overall change index for to the sample image.

It is apparent that a mere arithmetic average will be unduly skewed by these undesirably high values. Simply using the median would eliminate the disturbance altogether but at the same time remove an unacceptable number of higher indices that indicate actual erosion in their corresponding segment.

Our algorithm hence uses a count based index generation (Yang et al., 2013). We consider each available segment change index and count only those that exceed a certain

threshold. This threshold can be adjusted for different assignments as needed, but in our tests we consistently found 50 to be a practical value. The resulting occurrence count is reported as the overall change index for the corresponding image in the overall sample series.

This final step results in a time series data point that can easily be plotted over the entire observation period or any desired smaller timeframe. As our original image series only contains pictures from the two hour periods around each high tide, the resulting graph shows relatively few data points. This is further exacerbated by the fact that certain high tides occur at night and the images from others may be unusable due to lighting conditions, obscurations, camera defects or other adverse external effects. The resulting plot would hence be a very sparsely populated scatter plot that would not be of great use for the intended audience as the erosion data will be compared with other more frequently observed and reported data streams. To maintain compatibility with these streams we interpolate the erosion index into a continuous graph as illustrated in figure 15.

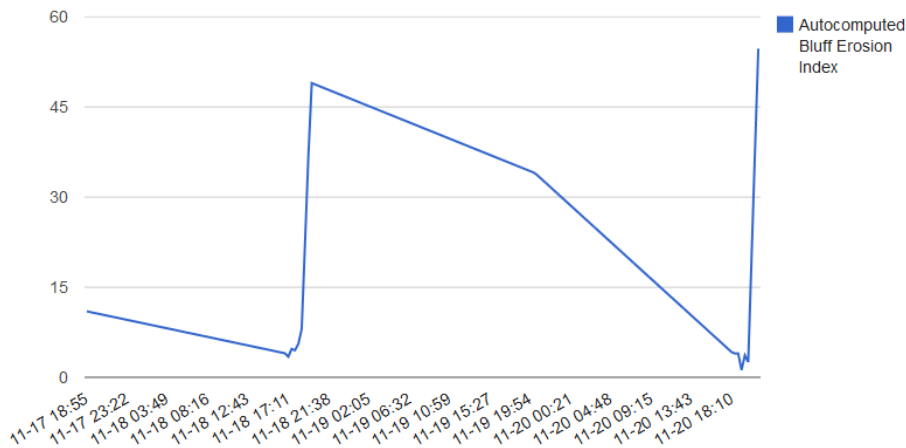


Figure 15: Interpolated Erosion Index Graph

CHAPTER III

RESULTS

Plottable Index

As we have stated before, the final goal of this study is to derive and generate an index that can be used to analyze the occurrence and intensity of erosion events in respect to other environmental influences. Future studies may well rely on this index in their correlation or regression analyses and while these are not part of our work, we can certainly show that our index can now be plotted against other existing data for the same time period. Consider, for example, the wind gust readings from the weather station located atop the main campus building on Thompson Island. Figure 16 not only shows the two graphs plotted alongside each other, but immediately appears to suggest a certain correlation. The latter will, of course, need to be proven in a separate study. It should be noted that when no erosion data is available, the index defaults to zero. This explains the unexpectedly flat line in the morning of November 21st.

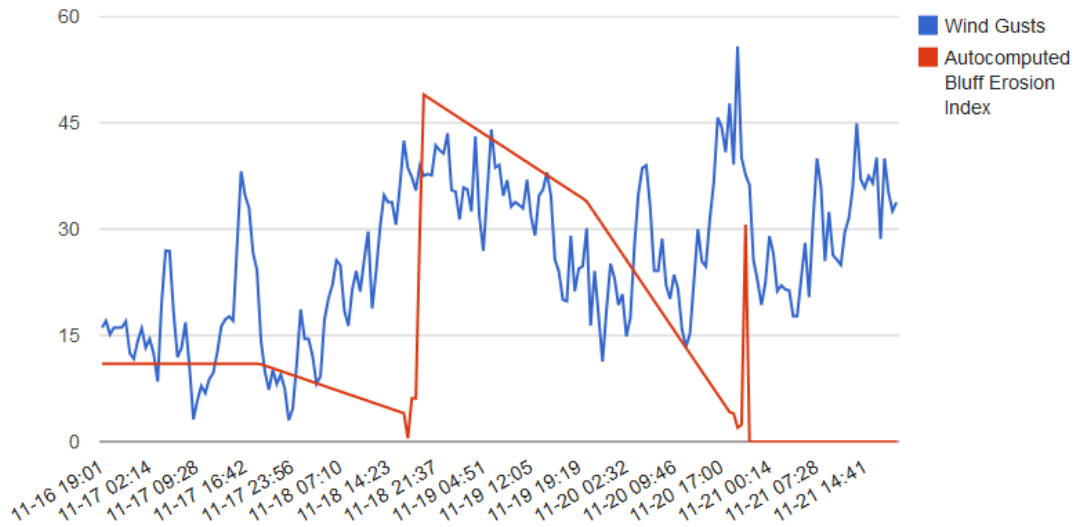


Figure 16: Erosion Index and Wind Gusts

Accuracy

Erosion events can be defined and classified in a multitude of ways which makes an entirely objective test of accuracy impossible. We can, however, compare our reported index to the subjective observations reported by individuals assisting in the visual inspection of all images in the series. To facilitate this measurement, we define two lists of events - Table 1 contains those that were observed by the human audience and table 2 lists those only indicated by our erosion index.

Table 1 shows that out of the fifteen actual erosion events that occurred during the observation period, our automated analysis correctly identified ten. This represents a rather impressive true positive rate of 67%. In addition to the fifteen actual events, the index also erroneously indicates the existence of four additional events shown in table 2.

Table 1: Actual Erosion Events

Event Start	Event End	Detected ?
11/20/14 7:20 PM	11/23/14 8:25 PM	No
11/23/14 9:45 PM	11/24/14 9:10 PM	Yes
11/24/14 10:00 PM	11/25/14 9:47 PM	Yes
11/25/14 11:07 PM	11/27/14 11:40 PM	Yes
11/28/14 12:50 AM	11/30/14 1:39 AM	Yes
12/1/14 4:39 PM	12/2/14 4:18 PM	No
12/2/14 4:58 PM	12/3/14 5:15 PM	Yes
12/3/14 5:25 PM	12/4/14 7:18 PM	Yes
12/5/14 8:18 PM	12/6/14 7:45 PM	Yes
12/6/14 9:05 PM	12/7/14 8:30 PM	Yes
12/7/14 9:50 PM	12/8/14 9:07 PM	No
12/8/14 9:37 PM	12/13/14 12:11 AM	Yes
12/16/14 4:36 PM	12/19/14 5:52 PM	No
12/19/14 6:22 PM	12/25/14 11:14 PM	Yes
12/31/14 4:18 PM	1/27/15 2:44 AM	No

Table 2: False Positives

Event Start	Event End
11/18/14 5:23 PM	11/18/14 6:33 PM
12/7/14 9:00 PM	12/7/14 9:20 PM
12/27/14 12:54 AM	12/28/14 12:15 AM
12/28/14 1:52 AM	12/29/14 1:32 AM

False positives can be caused by a wide variety of disturbances. Figure 17 compares the images before and after the first false positive. It is evident that no erosion has occurred, but a large number of leaves have been deposited - presumably by a mild wind gust. The red ellipse marks a particularly noticeable deposit. This change is subtle

enough to pass through our preprocessing steps and yet strong enough to register as a significant event.



Figure 17: Example of a False Positive

Using a basic single camera it is not possible to distinguish leaves from small rocks that could have been exposed by soil erosion. Therefore, such false positives cannot fully be avoided. However, the number of these cases is not particularly concerning when one considers the length of the observational period and the much larger number of actual events in that timeframe.

Statistical Significance

In addition to testing the index against human observations, we can also analyze potential correlations with a set of environmental data streams that were by the weather station located atop Thompson Island's main campus building. Some of these measurements are known to be indicative of erosion inducing microclimates. This, for

example, holds true for wind speeds and particularly wind gusts (Arnalds, Gisladdottir, & Orradottir, 2012) as well as precipitation rates (Blodgett & Isacks, 2007). Unfortunately the deployed hardware does not reliably record the latter. We do, however, have a breadth of other measurement available. Table 3 illustrates that at least five of these observations are significantly correlated with the computed erosion index. This includes both wind speed and wind gusts which strongly suggests that the index is indeed a valid measure of erosion events.

Table 3: Statistical Significance

	P-Value	Coefficient
Rel. Humidity	0.007064	-0.1106
Wind Speed	0.004931	0.2580
Wind Gusts	0.001963	0.1961
Temperaure	0.001247	-0.2159
Dew Point	0.000062	-0.2644

CHAPTER IV

DISCUSSION

Results

We have demonstrated that an image series obtained using a single stationary low cost consumer grade digital camera can be used to detect bluff erosion using only the visible light spectrum. It has become apparent that in order to quantify the intensity of observed erosions, one must isolate them from a large number of extrinsic disturbances such as changing tidal phases, wave motions, dominant sunlight and camera malfunctions.

We have been able to achieve better than anticipated results using an image segmentation technique that divides each image into square chunks. Erosion events were detected with a true positive rate of 67% while a relatively small number of false positives occurred. This excellent result can be explained by the fact that each subsegment of the original image is immune against disturbances such as sun rays or wave motion that may occur in other parts of the image. In addition to the improved

results, segmentation also allows for significant performance gains as the resulting segment series can be processed in parallel.

Finally we have stored and plotted the resulting erosion index alongside existing environmental data which suggests certain correlations between erosion events and meteorological influences such as wind gusts. We are confident that this method will form a solid basis for further research into coastal or bank erosion and that it will reduce the cost of data acquisition for researchers in various related fields.

Application

Most immediately, we suggest that interested parties employ our method to discover potential correlations between meteorological data and erosion event within the observed area. In this context it is particularly interesting whether such correlations exist between geographically disconnected data sources and - most importantly - whether one can show such correlations between past meteorological data and present erosion events. Such a correlation could be used to derive an erosion forecast based on current weather data and hence help coastal communities better assess the risk of impending erosions. Knowing which stretches of coastline or river banks may be at risk will allow for better disaster preparedness and facilitate the proper response to significant erosion events.

Further Research

As our method uses simple visual spectrum image series obtained with regular consumer grade digital cameras, it might also be adapted for entirely different purposes.

In our analysis, we break down an image into smaller segments, analyze each segment with the goal of detecting motion and then finally quantify the overall motion within the image in order to report a change index. This works quite well for erosion, but could certainly be equally useful to detect other small scale changes that occur over longer periods of time. Researchers might, for example, be interested in monitoring algae growth in lakes using a camera mounted at a certain elevation - possibly on a pole, an existing structure or, where permissible, on natural features such as trees.

Our method might also be useful for more complicated analyses such as the long term development of plant health. The different reflectivities of healthy and unhealthy vegetation is well documented and understood (Nijland et al., 2014), hence interested parties could use visual spectrum cameras or - where available - infrared spectrum cameras to create panoramic image series and monitor long term change that can, for example, be used to find correlations with climate change data. Aside from plant health, the spread of invasive species can be monitored in the same way (Müllerová, Pergl, & Pyšek, 2013).

The concept of tracing and quantifying small scale changes is highly transferrable and hence makes our method an extremely useful tool for a wide variety of scientific applications. However, our most immediate focus is on the monitoring and forecasting of erosion threats along the world's rivers banks, lake shores and coastlines. This, we hope, will result in reduced cost for communities and maybe even help to save human lives.

BIBLIOGRAPHY

- Aleksandrowicz, S., Turlej, K., Lewiński, S., & Bochenek, Z. (2014). Change detection algorithm for the production of land cover change maps over the European union countries. *Remote Sensing*, 6(7), 5976–5994. <http://doi.org/10.3390/rs6075976>
- An, X., Gong, H., McLoughlin, N., Yang, Y., & Wang, W. (2014). The mechanism for processing random-dot motion at various speeds in early visual cortices. *PLoS ONE*, 9(3). <http://doi.org/10.1371/journal.pone.0093115>
- Arnalds, O., Gísladóttir, F. O., & Orradóttir, B. (2012). Determination of aeolian transport rates of volcanic soils in Iceland. *Geomorphology*, 167–168, 4–12. <http://doi.org/10.1016/j.geomorph.2011.10.039>
- Ashique, K., & Kaliyadan, F. (2011). Clinical photography for trichology practice: tips and tricks. *International Journal of Trichology*, 3(1), 7–13. <http://doi.org/10.4103/0974-7753.82118>
- Ayana, E. K., Worqlul, A. W., & Steenhuis, T. S. (2015). Evaluation of stream water quality data generated from MODIS images in modeling total suspended solid emission to a freshwater lake. *Science of the Total Environment*, 523, 170–177. Retrieved from 10.1016/j.scitotenv.2015.03.132
- Barsanti, M., Calda, N., Valloni, R., Di Paola, G., Iglesias, J., Rodríguez, G., ... Pappone, G. (2011). Estimating Coastal Vulnerability in a Meso-Tidal Beach by Means of Quantitative and Semi-Quantitative Methodologies. *Journal of Coastal Research*, 61(61), 303–308. <http://doi.org/10.2112/SI61-001.1>
- Beilicci, E., Beilicci, R., & Ștefanescu, C. (2014). ASPECTS OF OPTIMIZATION OF SOIL EROSION CONTROL SYSTEMS. *Research Journal of Agricultural Science*, 46(1), 26–34. Retrieved from <http://search.ebscohost.com/login.aspx?direct=true&db=a9h&AN=99531033&site=ehost-live>
- Bejinariu, S. I., Costin, H., Rotaru, F., Luca, R., & Nit, C. (2014). Parallel Processing and Bio-inspired Computing for Biomedical Image Registration, 22(2), 253–278.

- Benabbas, Y., Ihaddadene, N., & Djeraba, C. (2011). Motion pattern extraction and event detection for automatic visual surveillance. *Eurasip Journal on Image and Video Processing*, 2011. <http://doi.org/10.1155/2011/163682>
- Bisquert, M., Bordogna, G., Bégué, A., Candiani, G., Teisseire, M., & Poncelet, P. (2015). A Simple Fusion Method for Image Time Series Based on the Estimation of Image Temporal Validity. *Remote Sensing*, 7(1), 704–724. <http://doi.org/10.3390/rs70100704>
- Blodgett, T. a., & Isacks, B. L. (2007). Landslide Erosion Rate in the Eastern Cordillera of Northern Bolivia. *Earth Interactions*, 11(19), 1–30. <http://doi.org/10.1175/2007EI222.1>
- Boak, E. H., & Turner, I. L. (2005). Shoreline Definition and Detection: A Review. *Journal of Coastal Research*, 214, 688–703. <http://doi.org/10.2112/03-0071.1>
- Buckler, W. R., & Winters, H. A. (1983). Lake Michigan Bluff Recession. *Annals of the Association of American Geographers*, 73(1), 89–110. Retrieved from <http://search.ebscohost.com/login.aspx?direct=true&db=sih&AN=12978718&site=ehost-live>
- Caradot, N., Granger, D., Chappier, J., Cherqui, F., & Chocat, B. (2011). Urban flood risk assessment using sewer flooding databases. *Water Science & Technology*, 64(4), 832. <http://doi.org/10.2166/wst.2011.611>
- Carpenter, D. W., Jung, R. E., & Sites Jr, J. W. (2001). Conservation genetics of the endangered Shenandoah salamander [Plethodon shenandoah, Plethodontidae]. *Animal Conservation*, 4(2), 111–119. Retrieved from <http://search.ebscohost.com/login.aspx?direct=true&db=ffw&AN=901741&site=ehost-live>
- Castedo, R., Fernández, M., Trenhaile, A. S., & Paredes, C. (2013). Modeling cyclic recession of cohesive clay coasts: Effects of wave erosion and bluff stability. *Marine Geology*, 335, 162–176. <http://doi.org/10.1016/j.margeo.2012.11.001>
- Cheng, G., & Buckles, B. P. (2014). A nonparametric approach to region-of-interest detection in wide-angle views. *Pattern Recognition Letters*, 49, 24–32. <http://doi.org/10.1016/j.patrec.2014.05.019>
- Da Silva, A. M., Huang, C. H., Francesconi, W., Saintil, T., & Villegas, J. (2015). Using landscape metrics to analyze micro-scale soil erosion processes. *Ecological Indicators*, 56, 184–193.

- Dabojani, D., Mithun, D., & Kanti, K. K. (2014). River Change Detection and Bankline Erosion Recognition using Remote Sensing and GIS, *XIII*(1), 100–105.
- Dawson, S. a., & Evans, J. E. (2001). Geological causes of local variation in coastal bluff recession rates, northeast Ohio Shoreline of Lake Erie. *Environmental Geosciences*, 8(1), 1–20. <http://doi.org/10.1046/j.1526-0984.2001.008001001.x>
- Day, S. S., Gran, K. B., Belmont, P., & Wawrzyniec, T. (2013a). Measuring bluff erosion part 1: Terrestrial laser scanning methods for change detection. *Earth Surface Processes and Landforms*, 38(10), 1055–1067. <http://doi.org/10.1002/esp.3353>
- Day, S. S., Gran, K. B., Belmont, P., & Wawrzyniec, T. (2013b). Measuring bluff erosion part 2: pairing aerial photographs and terrestrial laser scanning to create a watershed scale sediment budget. *Earth Surface Processes and Landforms*, 38(10), 1068–1082. <http://doi.org/10.1002/esp.3359>
- Dronova, I., Gong, P., Wang, L., & Zhong, L. (2015). Mapping dynamic cover types in a large seasonally flooded wetland using extended principal component analysis and object-based classification. *Remote Sensing of Environment*, 158, 193–206. <http://doi.org/10.1016/j.rse.2014.10.027>
- Dupret, A., Verdant, A., Villard, P., & Mathias, H. (2011). Three Novell analog-domain algorithms for motion detection in video surveillance. *Eurasip Journal on Image and Video Processing*, 2011. <http://doi.org/10.1155/2011/698914>
- Dutta, J., Leahy, R. M., & Li, Q. (2013). Non-local means denoising of dynamic PET images. *PLoS ONE*, 8(12). <http://doi.org/10.1371/journal.pone.0081390>
- Eivazi, A., Kolesnikov, A., Junttila, V., & Kauranne, T. (2015). Variance-preserving mosaicing of multiple satellite images for forest parameter estimation: Radiometric normalization. *ISPRS Journal of Photogrammetry & Remote Sensing*, 105, 120–127. Retrieved from 10.1016/j.isprsjprs.2015.03.007
- Fisher, A. (2013). Cloud and cloud-shadow detection in SPOT5 HRG imagery with automated morphological feature extraction. *Remote Sensing*, 6(1), 776–800. <http://doi.org/10.3390/rs6010776>
- García-Mateos, G., Hernández-Hernández, J. L., Escarabajal-Henarejos, D., Jaén-Terrones, S., & Molina-Martínez, J. M. (2015). Study and comparison of color models for automatic image analysis in irrigation management applications. *Agricultural Water Management*, 151, 158–166.

- Guo, W., Rage, U. K., & Ninomiya, S. (2013). Illumination invariant segmentation of vegetation for time series wheat images based on decision tree model. *Computers & Electronics in Agriculture*, *96*, 58–66. Retrieved from 10.1016/j.compag.2013.04.010
- Huang, C. C., Pang, J., Zha, X., Zhou, Y., Su, H., & Li, Y. (2010). Extraordinary Floods of 4100-4000 a BP recorded at the Late Neolithic Ruins in the Jinghe River Gorges, Middle Reach of the Yellow River, China. *Palaeogeography, Palaeoclimatology, Palaeoecology*, *289*(1-4), 1–9. <http://doi.org/10.1016/j.palaeo.2010.02.003>
- Huang, X., Zhu, T., Zhang, L., & Tang, Y. (2014). A novel building change index for automatic building change detection from high-resolution remote sensing imagery. *Remote Sensing Letters*, *5*(8), 713–722. <http://doi.org/10.1080/2150704X.2014.963732>
- Islam, M., Sallu, S., Hubacek, K., & Paavola, J. (2014). Migrating to tackle climate variability and change? Insights from coastal fishing communities in Bangladesh. *Climatic Change*, *124*(4), 733–746. Retrieved from 10.1007/s10584-014-1135-y
- Jia, Z., Wang, H., Caballero, R., Xiong, Z., Zhao, J., & Finn, A. (2011). A two-step approach to see-through bad weather for surveillance video quality enhancement. *Proceedings - IEEE International Conference on Robotics and Automation*, 5309–5314. <http://doi.org/10.1109/ICRA.2011.5979596>
- Jorgenson, M. T., & Brown, J. (2005). Classification of the Alaskan Beaufort Sea Coast and estimation of carbon and sediment inputs from coastal erosion. *Geo-Marine Letters*, *25*(2-3), 69–80. <http://doi.org/10.1007/s00367-004-0188-8>
- Karamouz, M., & Nazif, S. (2013). Reliability Based Flood Management in Urban Watersheds Considering Climate Change Impacts. *Journal of Water Resources Planning and Management*, (October). [http://doi.org/10.1061/\(ASCE\)WR.1943-5452.0000345](http://doi.org/10.1061/(ASCE)WR.1943-5452.0000345)
- Kastens, J. H., Kastens, T. L., Kastens, D. L. A., Price, K. P., Martinko, E. A., & Lee, R.-Y. (2005). Image masking for crop yield forecasting using AVHRR NDVI time series imagery. *Remote Sensing of Environment*, *99*(3), 341–356. Retrieved from 10.1016/j.rse.2005.09.010
- Kastner, S., & Ungerleider, L. G. (2000). Mechanisms of Visual Attention in the Human Cortex. *Annual Review of Neuroscience*, *23*(1), 315. Retrieved from <http://search.ebscohost.com/login.aspx?direct=true&db=a9h&AN=5365392&site=ehost-live>

- Kinsey, K., Anderson, S. J., Hadjipapas, a., & Holliday, I. E. (2011). The role of oscillatory brain activity in object processing and figure-ground segmentation in human vision. *International Journal of Psychophysiology*, 79(3), 392–400. <http://doi.org/10.1016/j.ijpsycho.2010.12.007>
- Lai, A.-C., Chong, K.-K., Lim, B.-H., Ho, M.-C., Yap, S.-H., Heng, C.-K., ... King, Y.-J. (2015). A Generic Sun-Tracking Algorithm for On-Axis Solar Collector in Mobile Platforms. *AIP Conference Proceedings*, 1657(1), 1–6. Retrieved from 10.1063/1.4915163
- Lalonde, J.-F., Efros, A., & Narasimhan, S. (2012). Estimating the Natural Illumination Conditions from a Single Outdoor Image. *International Journal of Computer Vision*, 98(2), 123–145. Retrieved from 10.1007/s11263-011-0501-8
- Li, G., Han, X., Lin, W., & Wei, H. (2012). Periodic motion detection with ROI-based similarity measure and extrema-based reference selection. *IEEE Transactions on Consumer Electronics*, 58(3), 947–954. Retrieved from 10.1109/TCE.2012.6311341
- Liau, Y.-T. (2014). Hierarchical Segmentation Framework for Identifying Natural Vegetation: A Case Study of the Tehachapi Mountains, California. *Remote Sensing*, 6(8), 7276–7302. <http://doi.org/10.3390/rs6087276>
- Lucero, L. J., Fedick, S. L., Dunning, N. P., Lentz, D. L., & Scarborough, V. L. (2014). 3 Water and Landscape: Ancient Maya Settlement Decisions. *Archeological Papers of the American Anthropological Association*, 24(1), 30–42. Retrieved from 10.1111/apaa.12027
- Matias, A., Ferreira, O., Mendes, I., Dias, J. A., & Vila-Concejo, A. (2005). Artificial Construction of Dunes in the South of Portugal. *Journal of Coastal Research*, 21(3), 472–481. Retrieved from 10.2112/03-0047
- Moura, D., Gabriel, S., Gamito, S., Santos, R., Zugasti, E., Naylor, L., ... Martins, A. L. (2012). Integrated assessment of bioerosion, biocover and downwearing rates of carbonate rock shore platforms in southern Portugal. *Continental Shelf Research*, 38, 79–88. Retrieved from 10.1016/j.csr.2012.03.003
- Müllerová, J., Pergl, J., & Pyšek, P. (2013). Remote sensing as a tool for monitoring plant invasions: Testing the effects of data resolution and image classification approach on the detection of a model plant species *Heracleum mantegazzianum* (giant hogweed). *International Journal of Applied Earth Observation and Geoinformation*, 25(1), 55–65. <http://doi.org/10.1016/j.jag.2013.03.004>

- National Oceanic and Atmospheric Administration. (1998). Mitigating the impacts of coastal hazards. In *Year of the Ocean Discussion Papers*. U.S. Dept. of Commerce, NAOO. Retrieved from <http://search.ebscohost.com/login.aspx?direct=true&db=ffw&AN=FSLT-285073&site=ehost-live>
- Nijland, W., de Jong, R., de Jong, S. M., Wulder, M. a., Bater, C. W., & Coops, N. C. (2014). Monitoring plant condition and phenology using infrared sensitive consumer grade digital cameras. *Agricultural and Forest Meteorology*, *184*, 98–106. <http://doi.org/10.1016/j.agrformet.2013.09.007>
- Nnolim, U. A. (2015). Design and implementation of novel, fast, pipelined HSI2RGB and log-hybrid RGB2HSI colour converter architectures for image enhancement. *Microprocessors & Microsystems*, *39*(4/5), 223–236.
- Ondimu, S. N., & Murase, H. (2008). COMPARISON OF PLANT WATER STRESS DETECTION ABILITY OF COLOR AND GRAY-LEVEL TEXTURE IN SUNAGOKE MOSS. *Transactions of the ASABE*, *51*(3), 1111–1120.
- Paganelli, C., Peroni, M., Baroni, G., & Riboldi, M. (2013). Quantification of organ motion based on an adaptive image-based scale invariant feature method. *Medical Physics*, *40*(11), 111701. <http://doi.org/10.1118/1.4822486>
- Párraga, C. a., Troscianko, T., & Tolhurst, D. J. (2005). The effects of amplitude-spectrum statistics on foveal and peripheral discrimination of changes in natural images, and a multi-resolution model. *Vision Research*, *45*(25-26), 3145–3168. <http://doi.org/10.1016/j.visres.2005.08.006>
- Paterson, R. G., Luger, M. I., Burby, R. J., Kaiser, E. J., Malcom, H. R., & Beard, A. C. (1993). Costs and benefits of urban erosion and sediment control: The North Carolina experience. *Environmental Management*, *17*(2), 167–178. <http://doi.org/10.1007/BF02394687>
- Peltoniemi, J., Hakala, T., Suomalainen, J., & Puttonen, E. (2009). Polarised bidirectional reflectance factor measurements from soil, stones, and snow. *Journal of Quantitative Spectroscopy & Radiative Transfer*, *110*(17), 1940–1953. Retrieved from [10.1016/j.jqsrt.2009.04.008](http://doi.org/10.1016/j.jqsrt.2009.04.008)
- Portillo-Portillo, J., Sánchez-Pérez, G., Olivares-Mercado, J., & Pérez-Meana, H. (2014). Detección de Movimiento de Vehículos en Secuencias de Video Basados en la Diferencia Absoluta entre Fotogramas y la Combinación de Bordes. *Información Tecnológica*, *25*(5), 129–136. <http://doi.org/10.4067/S0718-07642014000500018>

- Prokop, A., Schön, P., Singer, F., Pulfer, G., Naaïm, M., Thibert, E., & Soruco, A. (2015). Merging terrestrial laser scanning technology with photogrammetric and total station data for the determination of avalanche modeling parameters. *Cold Regions Science & Technology*, *110*, 223–230. Retrieved from 10.1016/j.coldregions.2014.11.009
- Protection, F., & Brown, J. L. (2008). FLOOD PROTECTION: Netherlands Makes Way for Rising Waters. *Civil Engineering (08857024)*, *78*(6), 19–21. Retrieved from <http://search.ebscohost.com/login.aspx?direct=true&db=bth&AN=32540126&site=ehost-live>
- Rozanov, N. N. (2004). Optical detection of motion of an object with a refractive index coinciding with the refractive index of the surroundings. *Optics and Spectroscopy*, *96*(6), 938–939. <http://doi.org/10.1134/1.1771431>
- Schmitt, K., Albers, T., Pham, T. T., & Dinh, S. C. (2013). Site-specific and integrated adaptation to climate change in the coastal mangrove zone of Soc Trang Province, Viet Nam. *Journal of Coastal Conservation*, *17*(3), 545–558. Retrieved from <http://search.ebscohost.com/login.aspx?direct=true&db=ffw&AN=974257&site=ehost-live>
- Singh, S., Saini, A. K., Saini, R., Mandal, A. S., Shekhar, C., & Vohra, A. (2014). A novel real-time resource efficient implementation of Sobel operator-based edge detection on FPGA. *International Journal of Electronics*, *101*(12), 1705–1715.
- Smith, A. (1995). Beaches and tourism - an example of the results of a dramatic beach erosion episode: Gold Coast, Queensland, Australia. *Shore and Beach*, *63*(3), 7–8. Retrieved from <http://search.ebscohost.com/login.aspx?direct=true&db=ffw&AN=IOSD000268-13&site=ehost-live>
- Smith, D. P., Ruiz, G., Kvitek, R., & Lampietro, P. J. (2005). Semiannual patterns of erosion and deposition in upper Monterey Canyon from serial multibeam bathymetry. *Geological Society of America Bulletin*, *117*(9/10), 1123–1133.
- Soomere, T., Viška, M., Lapinskis, J., & Räämet, A. (2011). Linking wave loads with the intensity of erosion along the coasts of Latvia. *Lainekoormuse Ja Rannikuprotsesside Intensiivsuse Seosest Läänemere Idarannikul.*, *17*(4), 359–374. Retrieved from 10.3176/eng.2011.4.06
- Spaan, W. P., Winteraeken, H. J., & Riksen, M. J. P. M. (2006). Dutch policy and practices on erosion control: Then and now. *Derzeitige Und Künftige Niederländische Politik Und Praktiken Der Erosionsbekämpfung*, *52*(2), 233–241. Retrieved from 10.1080/03650340600603861

- Stedel, T., Bugan, R., Kipka, H., Pfennig, B., Fink, M., de Clercq, W., ... Helmschrot, J. (2015). Implementing contour bank farming practices into the J2000 model to improve hydrological and erosion modelling in semi-arid Western Cape Province of South Africa. *Hydrology Research*, 46(2), 192. <http://doi.org/10.2166/nh.2013.164>
- Tang, Y., Mu, W., Zhao, L., & Zhao, G. (2014). An image segmentation method based on maximizing fuzzy correlation and its fast recursive algorithm. *Computers & Electrical Engineering*, 40(3), 833–843. Retrieved from 10.1016/j.compeleceng.2013.07.009
- Tenbrinck, D., & Jiang, X. (2015). Image segmentation with arbitrary noise models by solving minimal surface problems. *Pattern Recognition*, 48(11), 3293–3309. Retrieved from 10.1016/j.patcog.2015.01.006
- Teng, W.-G., & Chang, P.-L. (2012). Identifying Regions of Interest in Medical Images Using Self-Organizing Maps. *Journal of Medical Systems*, 36(5), 2761–2768. Retrieved from 10.1007/s10916-011-9752-8
- Van Staveren, M. F., Warner, J. F., van Tatenhove, J. P. M., & Wester, P. (2014). Let's bring in the floods: de-poldering in the Netherlands as a strategy for long-term delta survival? *Water International*, 39(5), 686–700. Retrieved from 10.1080/02508060.2014.957510
- Vicente-Serrano, S., Cabello, D., Tomás-Burguera, M., Martín-Hernández, N., Beguería, S., Azorin-Molina, C., & Kenawy, A. (2015). Drought Variability and Land Degradation in Semiarid Regions: Assessment Using Remote Sensing Data and Drought Indices (1982–2011). *Remote Sensing*, 7(4), 4391–4423. <http://doi.org/10.3390/rs70404391>
- Wang, L., Ma, Y., Zomaya, A. Y., Ranjan, R., & Chen, D. (2015). A Parallel File System with Application-Aware Data Layout Policies for Massive Remote Sensing Image Processing in Digital Earth. *IEEE Transactions on Parallel & Distributed Systems*, 26(6), 1497–1508. Retrieved from 10.1109/TPDS.2014.2322362
- Wang, Y., Wang, C., & LIU, J. (2003). A mathematical morphological algorithm for edge detection in remotely sensed image [J]. *Journal of Chongqing University of Posts and Telecommunications*, 2.
- Yang, L., Smith, J. a., Wright, D. B., Baeck, M. L., Villarini, G., Tian, F., & Hu, H. (2013). Urbanization and Climate Change: An Examination of Nonstationarities in Urban Flooding. *Journal of Hydrometeorology*, 14(6), 1791–1809. <http://doi.org/10.1175/JHM-D-12-095.1>

- Yoonessi, A., & Zaidi, Q. (2010). The role of color in recognizing material changes. *Ophthalmic and Physiological Optics*, 30(5), 626–631. <http://doi.org/10.1111/j.1475-1313.2010.00722.x>
- Yue, H., Cai, K., Luo, B., Jin, Y., & Zeng, Z. (2015). Denoising and Segmentation of Digital Feather Image Using Mean Shift Algorithm, 13(1).
- Zhongli, M. A., Xiumei, L., & Jie, W. E. N. (2014). Image adaptive segmentation algorithm for unmanned surface vehicle targets. (English). *Journal of Harbin Institute of Technology. Social Sciences Edition / Haerbin Gongye Daxue Xuebao. Shehui Kexue Ban*, 46(7), 53–59. Retrieved from <http://search.ebscohost.com/login.aspx?direct=true&db=sih&AN=99890703&site=ehost-live>
- Zhu, S., Zhao, J., Guo, L., & Zhang, Y. (2013). Unsupervised Natural Image Segmentation via Bayesian Ying–Yang Harmony Learning Theory. *Neurocomputing*, 121, 532–539. Retrieved from 10.1016/j.neucom.2013.05.017
- Zhu, Z., & Wang, Y. (2012). A hybrid algorithm for automatic segmentation of slowly moving objects. *AEU: International Journal of Electronics & Communications*, 66(3), 249–254. Retrieved from 10.1016/j.aeue.2011.07.009